IOP Publishing Nanotechnology
Nanotechnology 32 (2021) 095206 (8pp) https://doi.org/10.1088/1361-6528/abcacc

Single-walled carbon nanotube membranes as non-reflective substrates for nanophotonic applications

Denis M Zhigunov[1], Daniil A Shilkin[2], Natalia G Kokareva[2], Vladimir O Bessonov[2,3], Sergey A Dyakov[1], Dmitry A Chermoshentsev[1,4], Aram A Mkrtchyan[1], Yury G Gladush[1], Andrey A Fedyanin[2] and Albert G Nasibulin[1,5]

[1] Skolkovo Institute of Science and Technology, Bolshoy Boulevard 30, bld. 1, 121205 Moscow, Russia
[2] Faculty of Physics, M. V. Lomonosov Moscow State University, Leninskie Gory 1, 119991 Moscow, Russia
[3] Frumkin Institute of Physical Chemistry and Electrochemistry, Russian Academy of Sciences, Moscow 119071, Russia
[4] Moscow Institute of Physics and Technology, 141700 Dolgoprudny, Russia
[5] Department of Chemistry and Materials Science, Aalto University, PO Box 16100, FI-00076, Finland

E-mail: d.zhigunov@skoltech.ru

Received 28 August 2020, revised 9 November 2020
Accepted for publication 16 November 2020
Published 7 December 2020

Abstract

We demonstrate that single-walled carbon nanotube (SWCNT) membranes can be successfully utilized as nanometer-thick substrates for enhanced visualization and facilitated study of individual nanoparticles. As model objects, we transfer optically resonant 200 nm silicon nanoparticles onto pristine and ethanol-densified SWCNT membranes by the femtosecond laser printing method. We image nanoparticles by scanning electron and bright-field optical microscopy, and characterize by linear and Raman scattering spectroscopy. The use of a pristine SWCNT membrane allows to achieve an order-of-magnitude enhancement of the optical contrast of the nanoparticle bright field image over the results shown in the case of the glass substrate use. The observed optical contrast enhancement is in agreement with the spectrophotometric measurements showing an extremely low specular reflectance of the pristine membrane ($\leqslant$0.1%). Owing to the high transparency, negligibly small reflectance and thickness, SWCNT membranes offer a variety of perspective applications in nanophotonics, bioimaging and synchrotron radiation studies.

Supplementary material for this article is available online

Keywords: carbon nanotube, free-standing thin films, scattering spectroscopy, Mie resonances, nanoparticle imaging

(Some figures may appear in colour only in the online journal)

1. Introduction

Optically resonant nanostructures made of high-index semiconductor materials, e.g. Si, Ge and GaAs, are in a focus of thorough research nowadays due to their ability to control light at the nanoscale [1–5]. Low absorption losses and pronounced Mie-type resonances, as characteristics of nanoparticles made of high refractive index materials, have been a driving force for the rapidly growing research in all-dielectric nanophotonics, aimed at getting benefits from the excitation of magnetic and electric multipole modes of the particles in the visible and near-IR spectral regions [6]. The performance of nanophotonic devices, however, usually suffers from a substrate holding the resonant structures. As a

result of the substrate presence, the quality factor of the resonances may be reduced and the control over the individual modes limited. These effects can be partly suppressed by embedding the resonant particles into low refractive index material [7, 8], or placing an index matching layer between the substrate and the structure [9]. Trapping nanoparticles in free space by means of optical tweezers allows one to eliminate the substrate effects completely, but this comes at the cost of lower stability and complicated experimental arrangement [10]. Recently, it has been reported that ultrathin carbon nanomembranes with a thickness of only 1 nm can be used as substrate material for plasmonic metasurfaces [11]. The dimensions of such nanomembranes are however limited to several hundred micrometers by the mechanical strength, and the transfer process onto a desired holder is not straightforward [12]. Thus, search of a widely scalable substrate that can be produced by a simple and rapid fabrication technique for the needs of nanophotonics is currently an urgent challenge.

Free-standing single-walled carbon nanotube (SWCNT) films (i.e. SWCNT membranes) possess a unique combination of electrical and optical properties. In particular, they demonstrate low sheet resistance $\leqslant 40\ \Omega/\mathrm{sq}$ at the transmittance up to 90% in the visible range, providing a high potential for a number of applications in optoelectronics and photovoltaics [13–17]. Such membranes can be produced by an aerosol chemical vapor deposition synthesis method, which allows one to fabricate a thin film of randomly oriented high-quality SWCNTs without any liquid chemistry procedures, in contrast to a commonly used vacuum-filtration approach involving a suspension preparation step [18]. The lateral size of free-standing SWCNT films is shown to reach several centimeters and can be further scaled up. Moreover, these films can be easily dry transferred onto practically any holding substrate [19]. However, in spite of their prevalence in electronics, to the best of our knowledge, SWCNT membranes have never been considered as substrates for nanophotonic applications, while conventional (non free-standing) carbon nanotube films decorated with noble metal nanoparticles have been already proposed as active substrates for surface-enhanced Raman scattering [20–22].

Here, we show that the SWCNT membranes can be used as advanced substrates to visualize and characterize individual nanoparticles. To illustrate the proposed concept Mie-resonant silicon nanoparticles (Si NPs) have been taken. Using scanning electron microscopy (SEM), bright field (BF) optical microscopy, linear and Raman scattering spectroscopy, we have performed a comparative study of similar-sized Si NPs deposited on either pristine and ethanol-densified SWCNT membranes or a cover glass. The demonstrated approach opens an avenue for applications in nanophotonics, live cell imaging and synchrotron studies.

2. Methods

2.1. Sample fabrication

SWCNTs were grown in the gas phase by ferrocene vapor decomposition in the atmosphere of CO. Aerosol SWCNTs were filtered from the gas phase and collected on a microporous filter forming a sparse uniform film of randomly oriented SWCNTs. These films were subsequently dry transferred over square openings with the size of 20×20 mm^2 to form a pristine free-standing film. One of the membranes was then densified by ethanol drop-casting and subsequent drying in air. Such a procedure allows one to compress the membrane in the out-of-plane direction and to increase its sheet conductivity and tensile strength [23]. Both pristine and ethanol-densified SWCNT membranes possess a transmittance of about 80% at 550 nm, which defines these membranes as almost the thinnest mechanically stable free-standing SWCNT films [19]. In the case of the densified membrane, its thickness can be estimated as 20 ± 7 nm on the basis of corresponding spectroscopic ellipsometry measurements [24], while for the pristine membrane this parameter is currently under study. The silicon nanoparticles were fabricated by means of the laser-induced transfer method, also referred to as femtosecond (fs) laser printing [25, 26], for details of the laser printing procedure see supporting information, section 1 (available online at stacks.iop.org/NANO/32/095206/mmedia). To be used as a donor, a 100 nm thick amorphous silicon (a-Si) film was deposited on a cover glass substrate by e-beam evaporation at room temperature using an ultra-high-vacuum growth system [27]. As a result of the printing procedure, Si NPs were deposited onto the SWCNT membranes and a reference cover glass substrate (a colourless borosilicate glass).

2.2. Optical and structural characterization

SEM of the Si NPs transferred on SWCNT membranes was performed in the high vacuum mode at an accelerating voltage of 30 kV. Optical imaging was realized using bright-field microscopy in the reflection geometry on an Olympus BX53M microscope equipped with an Olympus MPlanFL N $50\times/0.8$NA objective. All images were obtained with a fixed camera exposure of 25 ms. The scattering spectra of single Si NPs were measured in the forward-scattering geometry using a microscopic setup equipped with an Ocean Optics QEPro spectrometer; the details of the setup can be found elsewhere [28]. The particles were illuminated from the side of the substrate with the numerical aperture set to about 0.2. Raman spectra of single Si NPs were measured using a micro Raman setup Horiba Jobin Yvon LabRAM HR Evolution in the backscattering geometry with an excitation by the 632.8 nm line of a He–Ne laser. Transmittance and reflectance measurements were performed using an Agilent Cary 5000 spectrophotometer equipped with an integrating sphere. The diffuse reflectance was measured at a normal incidence, while the total reflectance was measured at an angle of incidence of $3°20'$. Ellipsometry for densified SWCNT free-standing

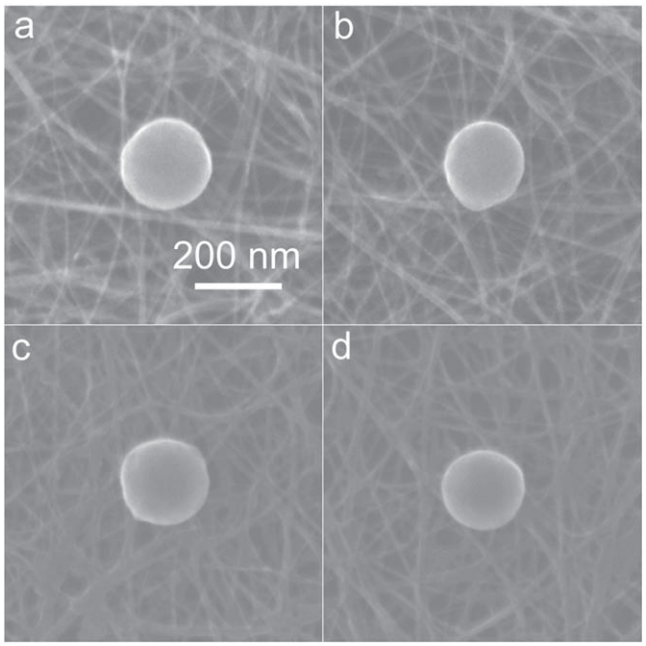

Figure 1. SEM images of Si NPs transferred on (a), (b) pristine and (c), (d) densified SWCNT membrane. Approximate size of the Si NPs is 210 nm (a), (c) and 190 nm (b), (d).

membranes was performed using spectroscopic ellipsometer Sentech Instruments SENresearch 4.0 in an angle range from 50° to 70°.

2.3. Numerical simulation

Numerical calculation of the scattering cross-section was performed using the finite element method in the commercial package COMSOL Multiphysics.

3. Results and discussion

Typical SEM images of the Si NPs on the pristine and ethanol-densified SWCNT membranes are shown in figure 1. The size of the printed NPs was found to vary between 190 and 220 nm due to variations of the fs laser pulse energy density (for additional SEM results see supporting information, section 2). All SEM images were obtained in high vacuum and without preliminary metal coating: the high electrical conductivity of SWCNT networks [13] provided an efficient charge drainage (note, that membranes are mixtures of 2/3 semiconducting and 1/3 metallic SWCNTs). At the same conditions, SEM visualization of the Si NPs on the glass substrate was not successful because of the charging of the sample. Thus, an important advantage of the SWCNT membranes is that their use allows one to eliminate charging during SEM studies, keeping at the same time the specimen in its virgin form.

A well-known optical imaging technique with enhanced optical contrast is dark-field microscopy. Due to resonant light scattering, size-dependent differently colored dark-field microscopic images of Si nanoparticles with the diameter of

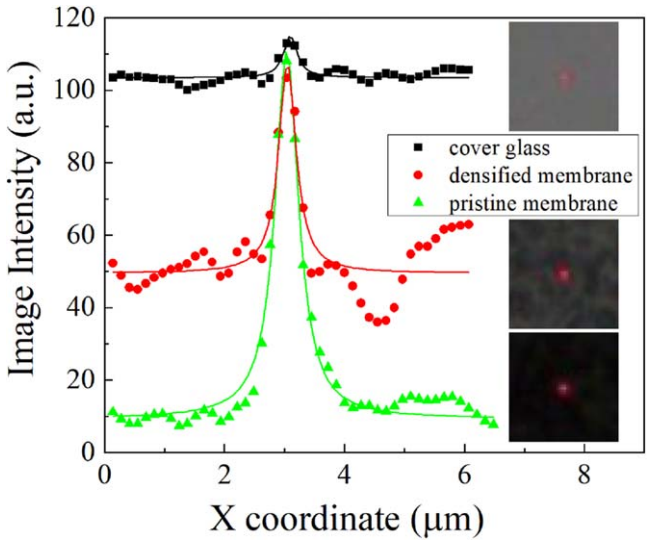

Figure 2. Intensity profiles (dots) taken along the horizontal median lines of the corresponding BF images (placed next to the curves) of the Si NPs transferred on different substrates. Solid lines represent a Lorentzian fit to the profiles.

~200 nm on a glass substrate can be easily obtained [29]. At the same time, visualization of such small particles using BF microscopy requires certain efforts aimed at the optical contrast enhancement: typically, high optical contrast is realized on low-reflectance substrates [30]. In this study, we reveal that pristine SWCNT membranes can be used for this purpose. Figure 2 shows BF microscopic images of individual Si NPs transferred on three different substrates—pristine and ethanol-densified SWCNT membranes and the cover glass; the corresponding signal intensity profiles taken from the median lines of the RGB images are shown as well. According to the obtained results, the best conditions for Si nanoparticle BF imaging are achieved, when the pristine SWCNT membrane is used, while the image of a particle on the cover glass substrate shows the lowest contrast due to an order-of-magnitude more intense background. Numerically, optical contrast, C, is defined as:

$$C = \frac{I_{NP} - I_{sub}}{I_{NP} + I_{sub}} \cdot 100\%, \quad (1)$$

where I_{NP} and I_{sub} represent image intensities, measured for Si NP (peak value) and adjacent substrate (average value), respectively. According to our data, Si NP image contrast increases from 7% ± 2% to 70% ± 12% if the cover glass substrate is replaced with a pristine SWCNT membrane (BF images of 20 different Si NPs were analyzed for averaging in each case; for more details see supporting information, section 3). In turn, images of Si NPs on the ethanol-densified SWCNT membrane show 29% ± 12% optical contrast due to a lighter background (see figure 2). Apparently, the enhanced contrast is caused by a much lower light reflectance from the SWCNT membranes in comparison with that of the cover glass. Similarly, conventional antireflective layers are used to achieve a better contrast in optical microscopy for the observation of 2D materials [30–32]. Hence, non-reflective SWCNT membranes seem to be perfect substrates for an

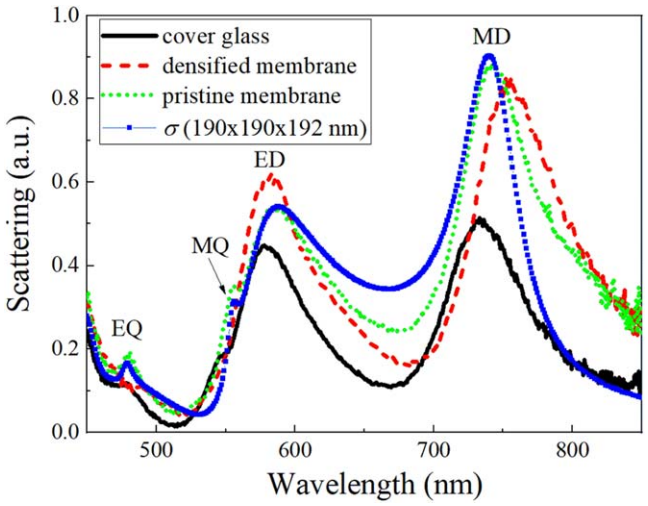

Figure 3. Scattering spectra of ∼190 nm Si NPs transferred onto different substrates: glass, pristine and densified SWCNT membrane (corresponding SEM images of Si NPs on SWCNT membranes are shown in figures 1(b) and (d)). For a comparison, calculated scattering cross-section, σ, is plotted for a 190 × 190 × 192 nm^3 spheroid.

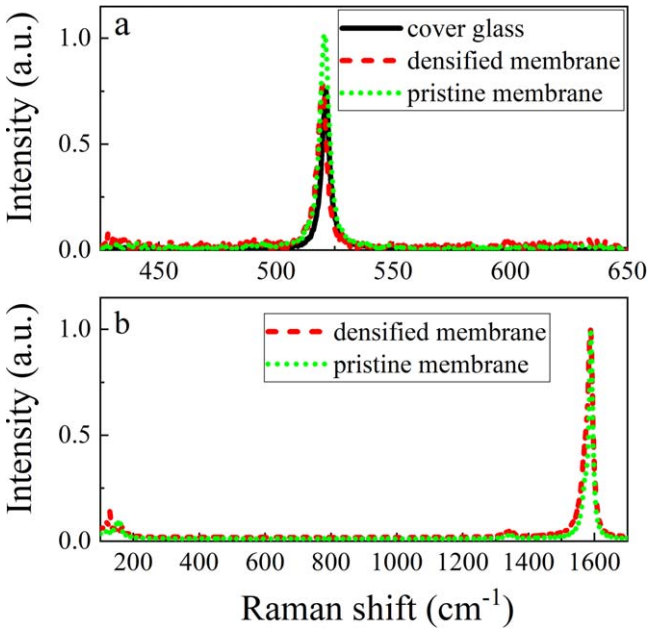

Figure 4. Raman spectra of (a) Si NPs transferred on a cover glass and SWCNT membranes (substrate-related background is subtracted), and (b) pure SWCNT membranes under study.

optical detection and characterization of various low-contrast specimens such as live cells, which are usually poorly detectable by BF optical microscopy [33].

Comparative linear and Raman scattering spectroscopy measurements were performed for single Si NPs (∼190 nm in size) transferred on the studied substrates. The results of the linear scattering spectroscopy are shown in figure 3. The obtained spectra of the Si NPs demonstrate pronounced resonances, which correspond to the excitation of magnetic dipole and electric dipole modes [29]. These resonances determine the color of the Si NPs, which can be seen in the corresponding BF images (see figure 2). The less pronounced high-order modes—electric quadrupole and magnetic quadrupole—are also distinguishable in the scattering spectra. The optically negligible thickness of the membranes may allow one to use them in studies of morphology-dependent optical resonances with the minimized substrate effects. In our study, however, the differences in size and shape of similar-sized but still individual Si NPs cause variations in the position and intensity of the observed scattering peaks, with no reliable effect of the substrate type on the scattering spectra established (for additional scattering spectroscopy results and comparison of spectra from different NPs see supporting information, section 4). The shown experimental spectra are in good agreement with the scattering cross-section calculated for a free-standing in air silicon spheroid with the major diameters 190 × 190 × 192 nm^3 as determined by the best fit of the scattering spectrum for the Si NP on the pristine SWCNT membrane. The results of the Raman spectroscopy, shown in figure 4(a), demonstrate that the transferred Si NPs are in a crystalline state, since only a narrow peak at ∼520 cm^{-1} characteristic for crystalline silicon is detected. The Raman spectra of the SWCNT films are almost featureless in the spectral region between 200 and 1300 cm^{-1} (see figure 4(b)), which provides the gap for Raman studies of different nanostructures being deposited on a film. During the measurements on the micro Raman setup, we found the high image contrast provided by the low-reflectance SWCNT substrates to significantly simplify a frequently complicated and time-consuming task of searching and positioning individual nanoparticles. Under certain experimental conditions, Si NPs on the glass substrate cannot be seen, in contrast to similar Si NPs on the SWCNT membranes (for details see supporting information, section 5). Relying on the presented results of comparative measurements, one may conclude that both pristine and densified SWCNT membranes are suitable substrates for the optical characterization of membrane-attached nanostructures.

In order to explain the observed BF image contrast enhancement upon using the free-standing SWCNT substrates, their optical properties have been studied. Figure 5 shows the transmittance and total reflectance of the SWCNT membranes in comparison with the cover glass, measured using an integrating sphere. The peaks around 280 nm in reflectance and the corresponding minima in transmittance for SWCNT membranes are explained by the well-known π-plasmon absorption [34], which leads to the increase in reflectance. Remarkably, the membranes demonstrate a high transmittance in the UV range (see figure 5(a)), which might be very useful for specific UV studies [35]. Moreover, the total reflectance of SWCNT membranes is much lower than that of the cover glass, showing a maximum of ∼1% at 275 nm for the pristine film (see figure 5(b)).

The obtained results demonstrate the outstanding non-reflective properties of pristine SWCNT membranes, which are closely comparable with those of well-known black silicon (reflectivity $\leqslant$1% [36]), and vertically aligned (VA) CNT arrays (reflectivity $\leqslant$0.1% [37]). Both of the latter materials

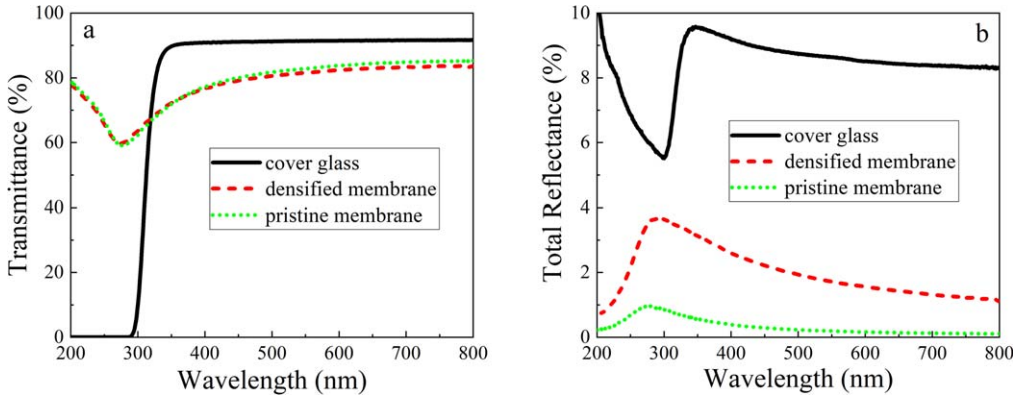

Figure 5. (a) Transmittance and (b) total reflectance of SWCNT membranes and a cover glass.

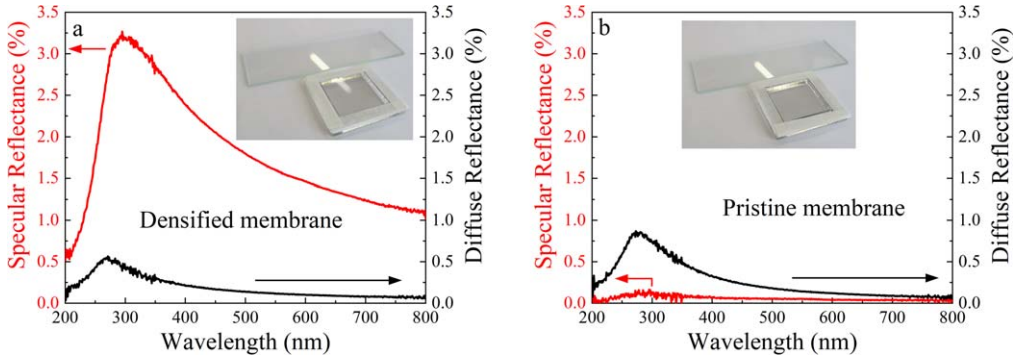

Figure 6. Specular and diffuse components of reflectance of (a) densified and (b) pristine SWCNT membranes. Insets: photo of SWCNT membranes taken under illumination of a daylight lamp; the glares from the lamp are clearly observable for the densified membrane and the reference slide glass.

represent a class of porous nanostructures containing the nanometer-sized features (pores, pillars or tubes), that are in a lateral direction much smaller than the light wavelength. Due to the low density of a porous layer (of any type), its effective refractive index becomes significantly lower than that of the corresponding bulk material, approaching the refractive index of air, which leads to a significant reduction of the reflectance. Moreover, the surface of a porous layer consists of a discontinuous random network that makes it much different from the optically smooth surfaces and decreases the specular light reflectance. Besides, the presence of a graded-density surface profile, typical for porous nanostructures, results in a blurred 'air-medium' interface, which provides a relatively smooth gradient of refractive index for the incident light [38]. The elimination of a sharp well-defined interface between the air and the porous film due to the graded-index surface is one of the basic principles of reflectance suppression, which is known for etched anti-reflective coatings from the 19th century [39].

SWCNT membrane is a porous low-density material with the pore size of the order of tens of nanometers, as evident both from the SEM images (see figure 1) and the measurements of the nanoparticle filtering efficiency [19]. Accordingly, an explanation of the low observed reflectance from the membranes lies in their porous nanostructure, possibly accompanied by the graded-index surface, as suggested during the analysis of the anti-reflection properties of SWCNT membranes covering a Si substrate [40]. At the same time, SWCNT membranes do not absorb light as much as discussed above black silicon and VACNT arrays, which are both known primarily as black absorbers. Hence, neither strong light absorption nor elongated 'light trapping' structure is necessary to obtain a non-reflective surface, which, in the extreme case, is a free-standing ultrathin film. Remarkably, the reflectance of the ethanol-densified SWCNT membrane is several times higher than that of the pristine one (see figure 5(b)). This is in full agreement with the background intensity difference for the BF microscopic images shown in figure 2. The higher reflectance of the densified membrane can be explained by the higher film density and, therefore, lower porosity. Consequently, an effective refractive index of the densified film is higher, and an interface between the air and the membrane is more abrupt, which leads to higher reflectance. A similar rise in reflectance has been reported recently for a VA multi-walled carbon nanotube forest, after its mechanical compression and surface modification by the nanotube tip bending towards horizontal orientation [41].

To distinguish the contributions from the specular and diffuse components of the SWCNT membrane total reflectance, we measured the diffuse reflectance by itself and subtracted it from the respective total reflectance spectra (see figure 6). It became clear then that the reflectance of the densified membrane is mostly specular with a minor contribution of the diffuse component (figure 6(a)). On the

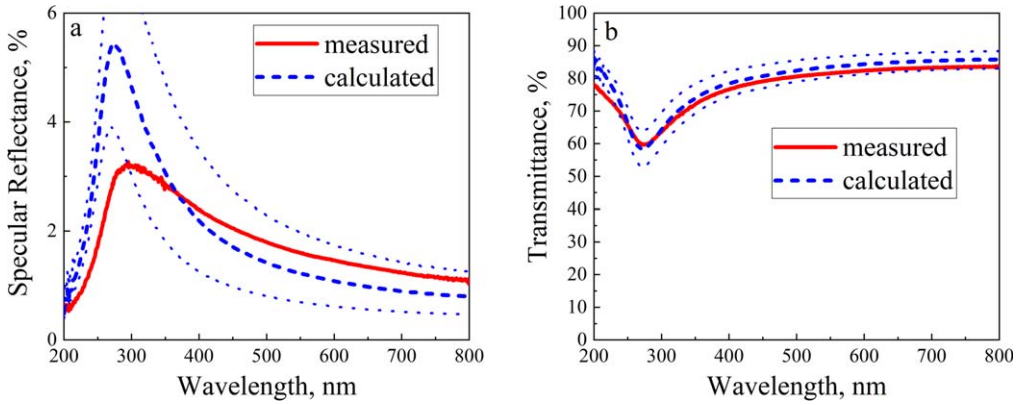

Figure 7. Measured and calculated spectra of (a) specular reflectance and (b) transmittance of densified SWCNT membrane under study. Dotted lines denote the range of calculation errors for the reflection and transmission spectra, which originate from the optical constants fitting errors as well as from the uncertainty of the membrane thickness.

contrary, the pristine membrane mostly scatters the light since the diffuse component dominates in the total signal, while the specular reflectance is extremely low: $\leqslant$0.1% (figure 6(b)). Hence, the pristine membrane may be classified as a practically perfect diffuse or so-called Lambertian reflector. We attribute such a negligibly small specular reflectance of the pristine membrane to its highly porous macrostructure accompanied by a graded-density surface profile, following the above discussion. The obtained $\sim$30-fold difference in the specular reflectance components correlates well with the naked eye observations: the pristine SWCNT membrane, being illuminated by the natural light, shows no glares at all, in contrast to the densified membrane and the reference slide glass (see insets in figures 6(a), (b)). At the same time, the diffuse components of the reflectance (i.e. scattering) are almost equal for both membranes. This is explained seemingly by the identical microstructure of SWCNTs composing the membranes, as well as by the nearly equal number of scattering centers, which is not altered significantly during the densification process. Herewith, a small rise of diffuse reflectance in the case of the pristine membrane, observed in figure 6, is caused presumably by its higher surface roughness in comparison with that of the densified membrane.

In relation to the BF microscopy, the image background is determined by both specular and diffuse reflectance of the substrate. The specular reflectance is dominant, but the diffuse one can also provide a significant contribution when a high-numerical aperture objective is used. The high optical contrast that we achieved using the pristine SWCNT membrane, is due to both the low diffuse and suppressed specular reflectance.

A simple model of a scalar complex local dielectric permittivity can be applied for the theoretical description of specular reflectance (R_s) and transmittance (T) of the densified SWCNT membrane in the wavelength range from near UV to infrared [42]. We have calculated R_s and T using dispersion relation of refractive index and extinction coefficient, determined from the ellipsometry data, by means of Fresnel equations (for additional details, see supporting information, section 6). The obtained satisfactory agreement between the measured and the calculated R_s and T (see figure 7) supports our assumption about the relatively smooth surfaces of the densified SWCNT membrane, which provide an abrupt interface between the air and the membrane. In contrast, for highly disordered pristine SWCNT membrane, the effects of spatial dispersion cannot be regarded as weak, and thus the model of a local dielectric permittivity is no longer applicable: we could not obtain a reasonable agreement between the measured and calculated spectra using neither scalar nor tensor of dielectric permittivity. An absence of abrupt interfaces, for which the Fresnel equations are usable, makes the quantitative description of interaction of the light with the pristine SWCNT membranes much more complicated.

It is worth noting that throughout the whole length of the study, the fabricated membranes remained intact. The mechanical strength of SWCNT membranes is comparable with that of common polymers such as polyethylene and nylon [19]. Together with the surprising durability of such nanometer-thick films, this allows one to manipulate freely with the experimental samples.

Finally, we propose to use the SWCNT membranes as substrates for x-ray and synchrotron radiation studies. There is a well-known issue with the Bragg coherent x-ray diffraction imaging of nanoscale systems, related to the spatial instability of nano-objects under intense x-ray beams [43]. The x-ray radiation induces charging of the substrates, which, together with the photon pressure of highly focused beams, is among the major contributions to rotation of sub-micron particles [44]. These problems can be potentially solved by employing the conductive SWCNT membranes as substrates for the x-ray measurements of a wide variety of nano-objects such as nanoparticles and nanowires. Furthermore, an important advantage of SWCNT membranes is their potential use in transmission geometry due to small film thickness leading to a minimized substrate contribution introduced by x-ray absorption and dynamical scattering effects.

4. Conclusion

In conclusion, we have proposed and demonstrated the application of SWCNT membranes as advanced nanometer-

thick substrates for visualization and characterization of individual Si NPs. The study has demonstrated that the high conductivity of both pristine and ethanol-densified SWCNT membranes facilitates the nanoparticle imaging by SEM. Due to the low optical reflectance of these membranes, they can be used as substrates in optical microscopy, providing at the same time sufficient gaps for Raman studies of nanostructures being deposited on a membrane. The optical contrast of the BF images of the Si NPs on the surface of the pristine SWCNT membrane has been shown to increase by an order of magnitude in comparison with the contrast obtained in the case of a glass substrate. Spectrophotometry of the pristine SWCNT membrane has revealed its extremely low reflectance in the UV, visible, and near-IR spectral ranges. It is found that the ethanol drop-casting densification procedure leads to a qualitative change in the character of SWCNT membranes reflection from almost perfect diffuse reflectance in the case of the pristine membrane toward predominantly specular reflectance for a densified one. Taking into account the negligibly small thickness and reflectance of the SWCNT membranes, their high transparency in the extreme UV range, and adjustable film thickness/transmittance, this type of substrates is expected to find applications in x-ray and synchrotron studies, which require minimization of substrate-related background and applicability for additional characterization techniques.

Acknowledgments

We are grateful to Alexander Ezhov, Evgeny Lyubin, Dmitry Dzhigaev and Ivan Filippov for their help with experiments and valuable suggestions. DMZ and DAS acknowledge the support of the Russian Foundation for Basic Research (Project No. 18-32-20217, optical microscopy measurements). DAS, NGK, VOB, AAF acknowledge the support of the Ministry of Education and Science of the Russian Federation (Project No. 14.W03.31.0008, fabrication of nanoparticles) and MSU Quantum Technology Center. DAS acknowledges the support of the Russian Science Foundation (Project No. 18-72-00247, linear scattering spectroscopy measurements). SAD and Yu GG thank Russian Foundation for Basis Research (Project No. 18-29-20032, simulation of optical properties). AGN acknowledges the support of Ministry of Education and Science of the Russian Federation (Project No. 0679-2020-0007 (FZSR-2020-0007) in the framework of state assignment No. 075-03-2020-097/1, SWCNT membrane fabrication).

ORCID iDs

Denis M Zhigunov https://orcid.org/0000-0003-1714-1208
Daniil A Shilkin https://orcid.org/0000-0001-7597-2734
Vladimir O Bessonov https://orcid.org/0000-0002-2165-1924
Sergey A Dyakov https://orcid.org/0000-0002-3729-6621
Yury G Gladush https://orcid.org/0000-0002-1289-2654
Albert G Nasibulin https://orcid.org/0000-0002-1684-3948

References

[1] Kuznetsov A I, Miroshnichenko A E, Brongersma M L, Kivshar Y S and Luk'yanchuk B 2016 Optically resonant dielectric nanostructures *Science* **354** aag2472
[2] Staude I and Schilling J 2017 Metamaterial-inspired silicon nanophotonics *Nat. Photon.* **11** 274–84
[3] Zyuzin M V, Baranov D G, Escudero A, Chakraborty I, Tsypkin A N, Ushakova E V, Kraus F, Parak W J and Makarov S V 2018 Photoluminescence quenching of dye molecules near a resonant silicon nanoparticle *Sci. Rep.* **8** 6107
[4] Grinblat G, Li Y, Nielsen M P, Oulton R F and Maier S A 2016 Enhanced third harmonic generation in single germanium nanodisks excited at the anapole mode *Nano Lett.* **16** 4635–40
[5] Shcherbakov M R *et al* 2017 Ultrafast all-optical tuning of direct-gap semiconductor metasurfaces *Nat. Commun.* **8** 17
[6] Krasnok A, Savelev R, Baranov D and Belov P 2017 *World Scientific Handbook of Metamaterials and Plasmonics, v. 1* 8 ed S Maier (Singapore: World Scientific) pp 337–85
[7] Staude I *et al* 2013 Tailoring directional scattering through magnetic and electric resonances in subwavelength silicon nanodisks *ACS Nano* **7** 7824–32
[8] Decker M, Staude I, Falkner M, Dominguez J, Neshev D N, Brener I, Pertsch T and Kivshar Y S 2015 High-efficiency dielectric huygens surfaces *Adv. Opt. Mater.* **3** 813–20
[9] Dong Z, Ho J, Yu Y F, Fu Y H, Paniagua-Dominguez R, Wang S, Kuznetsov A I and Yang J K W 2017 Printing beyond sRGB color gamut by mimicking silicon nanostructures in free-space *Nano Lett.* **17** 7620–8
[10] Andres-Arroyo A, Gupta B, Wang F, Gooding J J and Reece P J 2016 Optical manipulation and spectroscopy of silicon nanoparticles exhibiting dielectric resonances *Nano Lett.* **16** 1903–10
[11] Sirmaci Y D, Tang Z, Fasold S, Neumann C, Pertsch T, Turchanin A and Staude I 2020 Plasmonic metasurfaces situated on ultrathin carbon nanomembranes *ACS Photonics* **7** 1060–6
[12] Turchanin A and Gölzhäuser A 2016 Carbon nanomembranes *Adv. Mater.* **28** 6075–103
[13] Kaskela A *et al* 2010 Aerosol-synthesized SWCNT networks with tunable conductivity and transparency by a dry transfer technique *Nano Lett.* **10** 4349–55
[14] Hussain A, Liao Y, Zhang Q, Ding E-X, Laiho P, Ahmad S, Wei N, Tian Y, Jiang H and Kauppinen E I 2018 Floating catalyst CVD synthesis of single walled carbon nanotubes from ethylene for high performance transparent electrodes *Nanoscale* **10** 9752–9
[15] Tsapenko A P, Goldt A E, Shulga E, Popov Z I, Maslakov K I, Anisimov A S, Sorokin P B and Nasibulin A G 2018 Highly conductive and transparent films of $HAuCl_4$-doped single-walled carbon nanotubes for flexible applications *Carbon* **130** 448–57
[16] Mirri F, Ma A W K, Hsu T T, Behabtu N, Eichmann S L, Young C C, Tsentalovich D E and Pasquali M 2012 High-performance carbon nanotube transparent conductive films by scalable dip coating *ACS Nano* **6** 9737–44
[17] Rajanna P M, Meddeb H, Sergeev O, Tsapenko A P, Bereznev S, Vehse M, Volobujeva O, Danilson M, Lund P D and Nasibulin A G 2020 Rational design of highly efficient flexible and transparent p-type composite electrode

based on single-walled carbon nanotubes *Nano Energy* **67** 104183
[18] Gu H and Swager T M 2008 Fabrication of free-standing, conductive, and transparent carbon nanotube films *Adv. Mater.* **20** 4433–7
[19] Nasibulin A G *et al* 2011 Multifunctional free-standing single-walled carbon nanotube films *ACS Nano* **5** 3214–21
[20] Chen Y-C, Young R J, Macpherson J V and Wilson N R 2007 Single-walled carbon nanotube networks decorated with silver nanoparticles: a novel graded SERS substrate *J. Phys. Chem.* C **111** 16167–73
[21] Zhang X, Zhang J, Quan J, Wang N and Zhu Y 2016 Surface-enhanced Raman scattering activities of carbon nanotubes decorated with silver nanoparticles *Analyst* **141** 5527–34
[22] Basu S, Maulik S, Hou H-C, Daniels-Race T and Feldman M 2017 Surface enhanced Raman spectroscopic substrate utilizing gold nanoparticles on carbon nanotubes *J. Appl. Phys.* **122** 175107
[23] Wei Y, Jiang K, Feng X, Liu P, Liu L and Fan S 2007 Comparative studies of multiwalled carbon nanotube sheets before and after shrinking *Phys. Rev.* B **76** 045423
[24] Ermolaev G A, Tsapenko A P, Volkov V S, Anisimov A S, Gladush Y G and Nasibulin A G 2020 Express determination of thickness and dielectric function of single-walled carbon nanotube films *Appl. Phys. Lett.* **116** 231103
[25] Zywietz U, Evlyukhin A B, Reinhardt C and Chichkov B N 2014 Laser printing of silicon nanoparticles with resonant optical electric and magnetic responses *Nat. Commun.* **5** 3402
[26] Zhigunov D M, Evlyukhin A B, Shalin A S, Zywietz U and Chichkov B N 2018 Femtosecond laser printing of single Ge and SiGe nanoparticles with electric and magnetic optical resonances *ACS Photonics* **5** 977–83
[27] Drozdov M N, Drozdov Y N, Zakharov N D, Lobanov D N, Novikov A V, Yunin P A and Yurasov D V 2014 A new approach to the diagnostics of nanoislands in Ge_xSi_{1-x}/Si heterostructures by secondary ion mass spectrometry *Tech. Phys. Lett.* **40** 601
[28] Kroychuk M K, Shorokhov A S, Yagudin D F, Shilkin D A, Smirnova D A, Volkovskaya I, Shcherbakov M R, Shvets G and Fedyanin A A 2020 Enhanced nonlinear light generation in oligomers of silicon nanoparticles under vector beam illumination *Nano Lett.* **20** 3471–7
[29] Evlyukhin A B, Novikov S M, Zywietz U, Eriksen R L, Reinhardt C, Bozhevolnyi S I and Chichkov B N 2012 Demonstration of magnetic dipole resonances of dielectric nanospheres in the visible region *Nano Lett.* **12** 3749–55
[30] Huang F 2019 Optical contrast of atomically thin films *J. Phys. Chem.* C **123** 7440–6
[31] Jaouen K, Cornut R, Ausserré D, Campidelli S and Derycke V 2019 Ideal optical contrast for 2D material observation using bi-layer antireflection absorbing substrates *Nanoscale* **11** 6129–35
[32] Donnelly G E, Velický M, Hendren W R, Bowman R M and Huang F 2020 Achieving extremely high optical contrast of atomically-thin MoS_2 *Nanotechnology* **31** 145706
[33] Gutiérrez-Medina B and de Miranda M J S 2017 Quantitative image restoration in bright field optical microscopy *Biophys. J.* **113** 1916–9
[34] Kataura H, Kumazawa Y, Maniwa Y, Umezu I, Suzuki S, Ohtsuka Y and Achiba Y 1999 Optical properties of single-wall carbon nanotubes *Synth. Met.* **103** 2555–8
[35] Gubarev V M *et al* 2019 Single-walled carbon nanotube membranes for optical applications in the extreme ultraviolet range *Carbon* **155** 734–9
[36] Hsu C-H, Wu J-R, Lu Y-T, Flood D J, Barron A R and Chen L-C 2014 Fabrication and characteristics of black silicon for solar cell applications: an overview *Mater. Sci. Semicon. Proc.* **25** 2–17
[37] Yang Z-P, Ci L, Bur J A, Lin S-Y and Ajayan P M 2008 Experimental observation of an extremely dark material made by a low-density nanotube array *Nano Lett.* **8** 446–51
[38] Branz H M, Yost V E, Ward S, Jones K M, To B and Stradins P 2009 Nanostructured black silicon and the optical reflectance of graded-density surfaces *Appl. Phys. Lett.* **94** 231121
[39] Minot M J 1976 Single-layer, gradient refractive index antireflection films effective from 0.35 to 2.5 μ *J. Opt. Soc. Am.* **66** 515–9
[40] De Nicola F, Hines P, De Crescenzi M and Motta N 2016 Moth-eye effect in hierarchical carbon nanotube anti-reflective coatings *Carbon* **108** 262–7
[41] Mukherjee S and Misra A 2014 Broadband wavelength-selective reflectance and selective polarization by a tip-bent vertically aligned multi-walled carbon nanotube forest *J. Phys. D: Appl. Phys.* **47** 235501
[42] Afinogenov B I, Kopylova D S, Abrashitova K A, Bessonov V O, Anisimov A S, Dyakov S A, Gippius N A, Gladush Y G, Fedyanin A A and Nasibulin A G 2018 Midinfrared surface plasmons in carbon nanotube plasmonic metasurface *Phys. Rev. Appl.* **9** 024027
[43] Kim J W, Ulvestad A, Manna S, Harder R, Fohtung E, Singer A, Boucheron L, Fullerton E E and Shpyrko O G 2016 Observation of x-ray radiation pressure effects on nanocrystals *J. Appl. Phys.* **120** 163102
[44] Liang M, Harder R and Robinson I 2018 Radiation-driven rotational motion of nanoparticles *J. Synchrotron Radiat.* **25** 757–62